Journal of Vibration Engineering & Technologies (2021) 9:1175–1192
https://doi.org/10.1007/s42417-021-00289-8

ORIGINAL PAPER

A Coupled Model of Angular-Contact Ball Bearing–Elastic Rotor System and Its Dynamic Characteristics Under Asymmetric Support

Yi Liu[1,2] · Heng Liu[3]

Received: 15 January 2021 / Revised: 10 February 2021 / Accepted: 18 February 2021 / Published online: 15 June 2021

Abstract

This paper provides the dynamic model of an angular-contact ball bearing–elastic rotor system to study its dynamic characteristics when an asymmetric support mode is used. After defining global and local coordinate systems, necessary vectors (such as position, velocity, force and moment vector) are calculated according to the geometric relationship between each part (ball, cage and ring) of the bearing. The interactive forces between each part are obtained based on lubrication theory and Hertz contact theory. A typical rotor is discretized by finite element method (FEM) and each node of the rotor has 5 degrees of freedom (DOFs). Some constraint equations are built to form a coupled dynamic model of angular-contact ball bearing–elastic rotor system. The validity of this coupled model is verified by comparing the numerical results and experimental data. After analyzing the coupled model, it is found that the vibration spectrum of rotor includes the VC (varying compliance) frequencies of two bearings, the bending resonance frequency of rotor and the rotating frequency when the system has asymmetric ball bearings. Moreover, when the preloading forces of bearings increase, the support stiffness becomes larger and the rotor displacement decreases; moreover, the motions of balls and cage become more stable. Generally, the presented coupled model can be applied to analyze the vibration features of all parts in any ball bearing–rotor system comprehensively.

Keywords Ball bearing–rotor system · Coupled dynamic model · Vibration · Asymmetric support · Frequency

Introduction

Ball bearing–rotor system has been widely applied in the modern rotating machineries such as automobile, high-speed train, precision machine tool, wind power, aero-engine and so on. It is usually regarded as a kind of core component which have many advantages of high efficiency, reliable construction, convenient lubrication, high precision and excellent load capacity. The dynamic characteristics of ball bearing–rotor system directly decide the operational status, working life and security of the equipment.

✉ Heng Liu
hengliu@mail.xjtu.edu.cn

[1] Key Laboratory of Education Ministry for Modern Design and Rotor-Bearing System, Xi'an Jiaotong University, Xi'an, P. R. China

[2] State Key Lab for Strength and Vibration of Mechanical Structures, Xi'an Jiaotong University, Xi'an, P. R. China

[3] School of Mechanical Engineering, Xi'an Jiaotong University, Xi'an, P. R. China

The ball bearing–rotor system is basically a typical nonlinear multi-body dynamic system and there are coupling effects between the ball bearings and elastic rotor inevitably. Therefore, the essential mechanism of many phenomena such as the abnormal vibration of rotor and the premature failure of ball bearing has not been revealed. It is hard to distinguish whether rotor vibration causes bearing failure, or bearing failure causes the abnormal vibration of rotor. As a result, the research on the dynamic features of the ball bearing–rotor system especially on the coupling effects of the system is very important.

Based on the static and quasi-static theory, Perret [1] and Meldau [2] introduced the assumption of component rigidity and built the static model of deep groove ball bearing to discuss the varying compliance vibration (called VC vibration) of bearings with variable stiffness. Fukata et al. [3] established a nonlinear spring model of rolling bearings and discussed the sub-harmonic, super-harmonic and chaotic effects of the system. Based on this 2-DOFs nonlinear spring model, a large number of researchers have deeply studied the influences of rotation speed [4, 5], unbalanced force [6, 7], rolling body size [8] and other factors on the

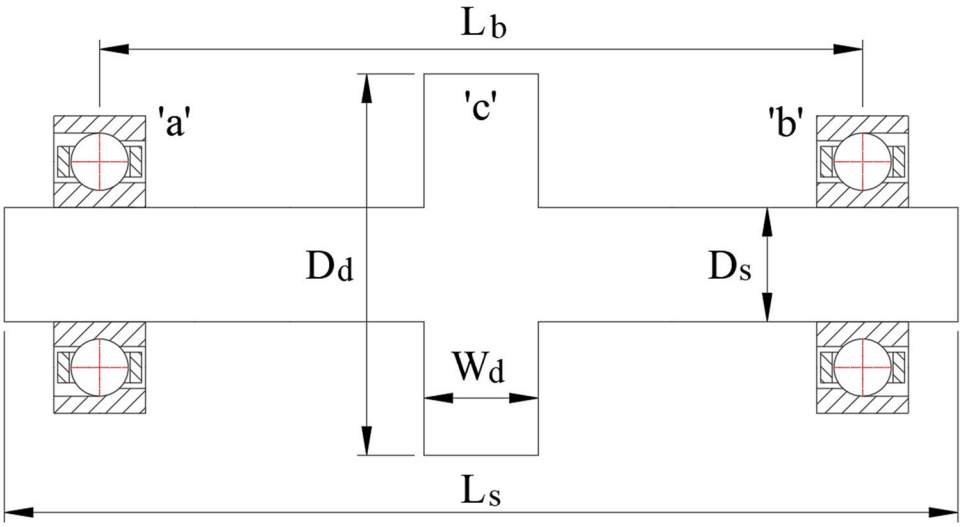

Fig. 1 Structure of classic ball bearing–elastic rotor system

nonlinear behavior of the system. Subsequently, Akturk et al. [9–11] took the axial motion of rotor into account, established a 3-DOFs model and studied the effects of preload, roller number and surface ripple. A 5-DOFs model, which includes the rotating angles, was proposed by Aini et al. [12] and applied to study the precise electric spindle system.

The model is improved by considering the gyroscopic motion, centrifugal force and other factors of rolling body. Sunnersjo [13] studied the inertia and damping effect of rolling body and the flexible vibration of bearing on the basis of the quasi-statics supporting model. Based on the Jones model, DeMul et al. [14] assembled the stiffness matrix of rolling bearing and rotor stiffness matrix to achieve coupling state. Cao and Altintas [15] not only established the finite element model of machine tool spindle using Timoshenko beam element with 5-DOFs but also built the dynamic model of machine tool spindle-bearing system which combined with the equivalent stiffness matrix of deep groove ball bearing. In these models, the inertia forces of cage and components are not included in the quasi-static model of rolling bearing, so the vibration characteristics of multiple components of the bearing are not considered, and the complex interaction force relations and motion characteristics between components cannot be truly reflected.

In recent years, it is a focus to build coupling system by combining the dynamic model of rolling bearing and rotor. Wensing [16] used finite elements to establish flexible rotor, rings and bearing housing after ignoring the cage. The interaction relationship between rolling body and inner ring was treated using linear spring which form the coupling dynamic model of deep groove ball bearing–rotor system to analyze the natural frequencies, modes and bearing vibration. Fritzson et al. [17] realized the motorized spindle system coupling dynamic model based on the transmission line principle (TLM). Among them, the elastic rotor model is established using finite element software and the rolling

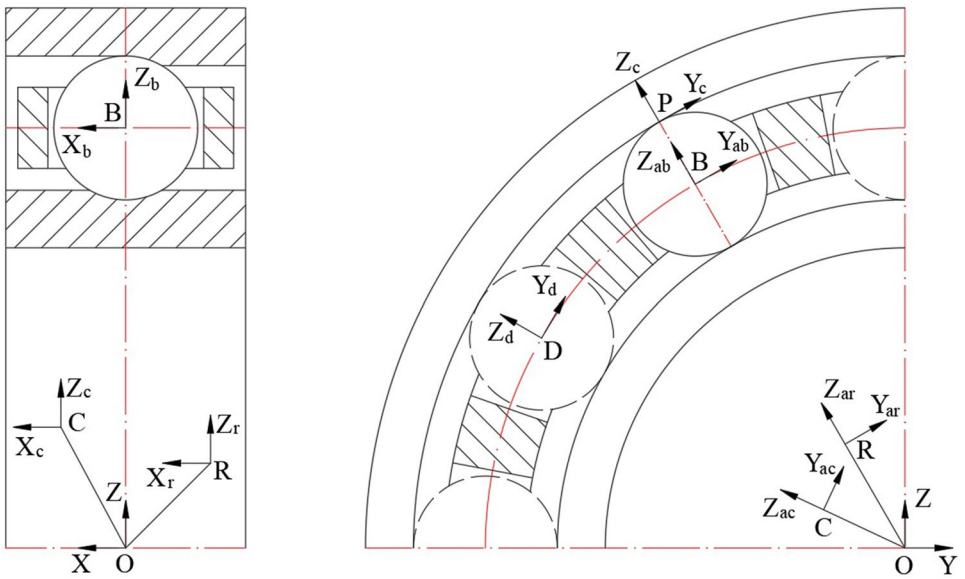

Fig. 2 Coordinate systems of ball bearing

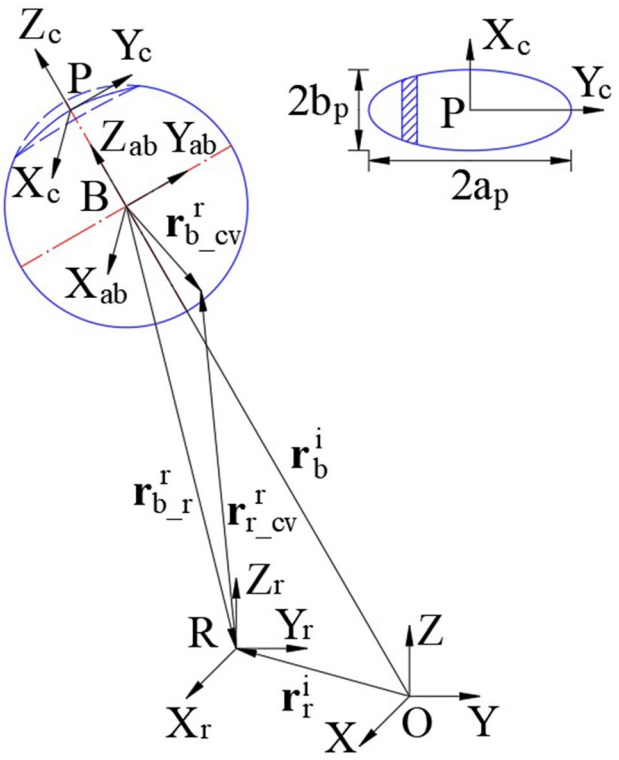

Fig. 3 Geometric relationship between ball and raceway

bearing model is built by multi-body dynamics analysis software. A certain time delay is introduced between the different components, resulting in a certain time difference between the component response of the rolling bearing and the rotor component response. Ashtekar [18] combined the finite element method and the discrete element method to establish a simulation model of squeeze film damper-angular-contact ball bearing-flexible rotor turbocharger, and carried out experimental verification.

However, it must also be recognized that there are still some limitations in the existing models. Therefore, it is a necessary way for the rolling bearing supporting rotor system mechanical model to get closer to the reality that establishes a fully dynamic rolling bearing supporting model combined with the dynamic response of flexible rotor and constitutes a system synchronous simulation analysis platform.

To study the comprehensive vibration features of all parts in any ball bearing system, this paper presents a feasible way to provide a coupled dynamic model of an angular-contact ball bearing–elastic rotor system which has the ability to investigate the dynamic characteristics of system when asymmetric bearings are used.

Coupled Dynamic Model of Angular-Contact Ball Bearing–Elastic Rotor System

Figure 1 depicts a classic ball bearing–rotor system. The rotor is composed of an elastic shaft and a rotating disk 'c'. The rotor is supported by two angular-contact ball bearings ('a' and 'b'). Every part of the ball bearings (balls, cages and rings) are all considered in dynamic analysis. Actually, the inner ring and shaft journal have interference fit. Therefore, the inner ring and rotor are assumed to be consolidated. The outer ring is immobilized and does not have any DOF. Two bearings can be identical or asymmetric ones. The basic parameters of structure, operation and load can be different. This ball bearing–elastic rotor system is a basic model and can be used in widespread conditions.

Dynamic Model of Angular-Contact Ball Bearing

Coordinate Systems and Basic Parameters

In a ball bearing, the relative position and sliding speed of each part (including ball, ring and cage) are the basis for obtaining their interactive force. Therefore, it is necessary to establish different coordinate systems (Fig. 2) to express multiple motion state and mutual forces for each part conveniently and accurately:

(1) Inertial coordinate system: origin O is set at the mass center of outer ring which is stationary when the angular-contact ball bearings are working; axis *X* coincides with the central axis of bearing; axis *Z* is the opposite

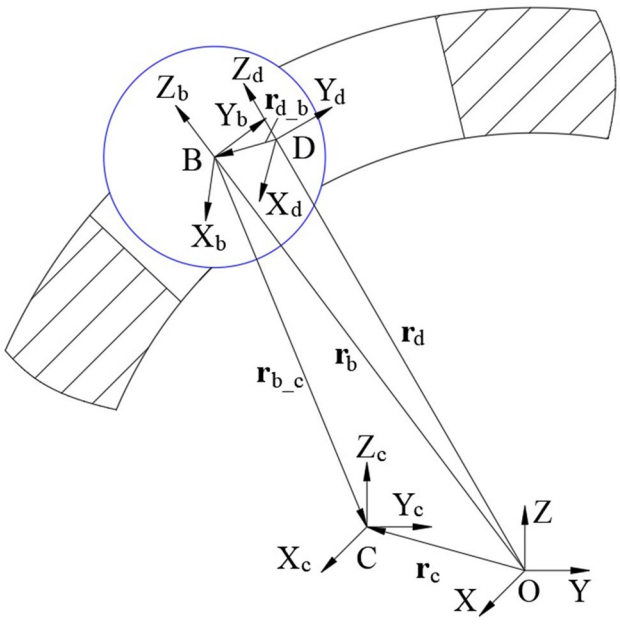

Fig. 4 Geometric relationship between ball and cage pocket

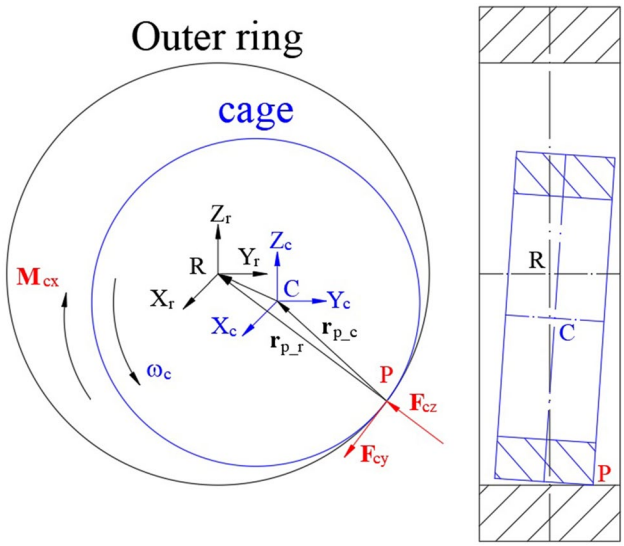

Fig. 5 Geometric relationship between outer ring and cage

direction of gravity; axis *Y* is determined according to the right hand rule.

(2) Body-fixed coordinate systems: $BX_bY_bZ_b$, $RX_rY_rZ_r$ and $CX_cY_cZ_c$ are the body-fixed coordinate systems for ball, inner ring and cage; *B*, *R* and *C* are the origins which are fixed on the mass center of each part; each axis directions coincide with the coordinate axis of inertial coordinate system, and then they are translated and rotated together with the corresponding part bodies.

(3) Other coordinate systems: $BX_{ab}Y_{ab}Z_{ab}$, $RX_{ar}Y_{ar}Z_{ar}$ and $CX_{ac}Y_{ac}Z_{ac}$ are the azimuth coordinate system of ball, ring and cage which describes the circumferential and radial position of each part; $PX_cY_cZ_c$ is the contact coordinate system which is used to analyze the contact state; $DX_dY_dZ_d$ is the pocket coordinate system which is applied to calculate the collision force between ball and pocket.

T_{m_n} is the transformation matrix from 'm' coordinate system to 'n' coordinate system. Subscript 'm' and 'n' can stand for inertial coordinate system ('*i*'), body-fixed coordinate systems ('b', 'r', 'c' for each part), azimuth coordinate systems ('a'), contact coordinate system('p'), pocket coordinate systems ('d') and other defined coordinate systems in use. $T_{m\_n}^{-1}$ represents the inverse transformation.

In a certain coordinate system 'm', parameters $\mathbf{r}_{d\_e}^{m}$ and $\mathbf{v}_{d\_e}^{m}$ are the position and velocity vector from part 'd' to part 'e' (subscript 'd' and 'e' can be 'b', 'r', 'c' for each part). If a part is in the inertial coordinate system, $\mathbf{r}_{d\_e}^{m}$ and $\mathbf{v}_{d\_e}^{m}$ can be simply described as $\mathbf{r}_d^{\,i}$ and $\mathbf{v}_d^{\,i}$. Parameters $\boldsymbol{\omega}_b^{\,b}$, $\boldsymbol{\omega}_c^{\,c}$, $\boldsymbol{\omega}_r^{\,r}$ represent the rotation speed vector of each part in the corresponding body-fixed coordinate system.

Interactive Force Between Ball and Ring

The relative geometric position between the ball and ring raceway is shown in Fig. 3. In the body-fixed coordinate system of ring, the azimuth angle of ball is θ_{br} and the position vector of the raceway curvature center in the direction of ball is expressed as

$$\mathbf{r}_{cv\_r}^{r} = \begin{pmatrix} 0 & -r_f \sin\theta_{br} & r_f \cos\theta_{br} \end{pmatrix}^T, \tag{1}$$

where r_f is the radius of curvature center locus circle of raceway.

In the azimuth coordinate system of ball, the position vector of ball center to curvature center of raceway is written as

$$\mathbf{r}_{b\_cv}^{a} = T_{i\_a}T_{i\_r}^{-1}\left(\mathbf{r}_{b\_r}^{r} - \mathbf{r}_{cv\_r}^{r}\right). \tag{2}$$

Then, the actual contact angle is written as

$$\begin{cases} \alpha_{c1} = \arctan\left(r_{b\_r1}^{a}/r_{b\_r3}^{a}\right) \\ \alpha_{c2} = \arctan\left[-r_{b\_r2}^{a}/\sqrt{\left(r_{b\_r1}^{a}\right)^2 + \left(r_{b\_r3}^{a}\right)^2}\right] \end{cases}, \tag{3}$$

with subscripts '1', '2', '3' meaning the projection of $\mathbf{r}_{b\_cv}^{a}$ in the direction of *X*, *Y* and *Z* axes.

Then, the transformation matrix from the azimuth coordinate system of ball to the contact coordinate system is $T_{ap} = T(\alpha_{c1}, \alpha_{c2}, 0)$, and the contact deformation between ball and ring raceway can be expressed as:

$$\delta_{br} = \left|\mathbf{r}_{b\_cv}^{a}\right| - \left(f_r - 0.5\right)d_b, \tag{4}$$

where f_r is the radius coefficient of groove curvature; d_b is the ball diameter.

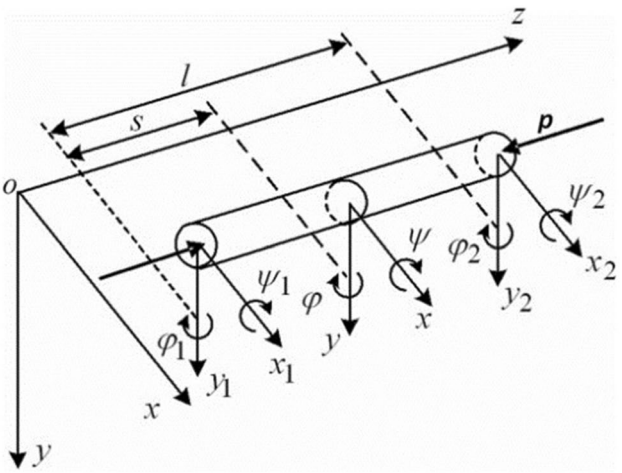

Fig. 6 Timoshenko beam element

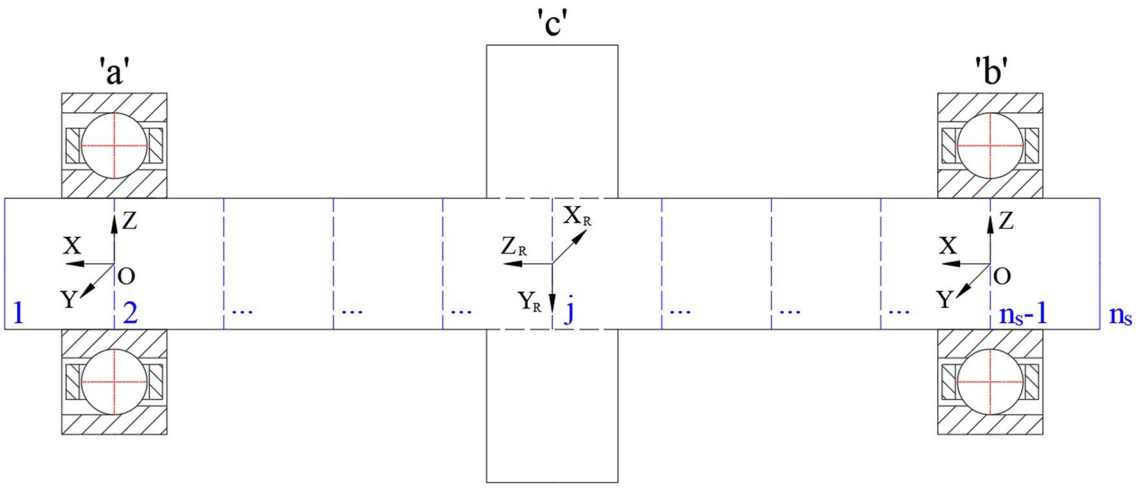

Fig. 7 The coupled dynamic model of ball bearing–rotor system

After the contact deformation is obtained, the elliptical contact area will appear at the contact between ball and raceway which is shown in Fig. 3. Hertz point contact theory is used to calculate the long half axis a_p, short half axis b_p and contact stress p_h. When the ellipse contact area is divided into several narrow strips, the position vector of contact point (on the narrow strip) relative to ball center is obtained as

$$\mathbf{r}_{p\_b}^{p}=\left(x_c,0,\sqrt{\overline{R}^2-x_c^2}-\sqrt{\overline{R}^2-a_p^2}+\sqrt{0.25d_b^2-a_p^2}\right)^T, \tag{5}$$

where $\overline{R}$ is the curvature radius of contact compression surface between ball and raceway; x_c is the coordinate value of contact point in x direction.

In the inertial coordinate system, the position vector of contact point relative to ring center is described as

$$\mathbf{r}_{p\_r}^{i}=T_{ia}^{-1}T_{ap}^{-1}\mathbf{r}_{p\_b}^{p}+\mathbf{r}_{b\_r}^{i}. \tag{6}$$

In the contact coordinate system, the sliding velocity vector of raceway relative to ball is

$$\mathbf{u}_{r\_b}^{p}=T_{a\_p}T_{i\_a}\left\{\mathbf{v}_r^i+\left[\left(T_{i\_r}^{-1}\boldsymbol{\omega}_r^r-\begin{pmatrix}\dot{\theta}_b\\0\\0\end{pmatrix}\right)\times r_{p\_r}^{i}\right]\right\} -T_{a\_p}\left[\begin{pmatrix}\dot{x}_b\\0\\\dot{r}_b\end{pmatrix}+\left(T_{i\_a}T_{i\_b}^{-1}\boldsymbol{\omega}_b^b\right)\times\left(T_{a\_p}^{-1}\mathbf{r}_{p\_b}^{p}\right)\right]. \tag{7}$$

After introducing $\mathbf{u}_{r\_b}^{p}$ into the formula of traction coefficients [19], the vector of traction coefficients is

$$\mathbf{k}_{b\_r}^{p}=T_{xc\_p}^{-1}\left(k_{b\_r1}\ \ k_{b\_r2}\ \ 0\right)^T. \tag{8}$$

In the contact coordinate system, the vector of force and moment acting on contact point of ball is shown as

$$\begin{cases}\mathrm{d}\,\mathbf{F}_{xc\_b}^{p}=p_h a_p b_p\sqrt{a_p^2-x_c^2}\left[\mathbf{k}_{b\_r}^{p}-(0,0,1)^T\right]\mathrm{d}x_c\\ \mathrm{d}\,\mathbf{M}_{xc\_b}^{p}=\mathbf{r}_{xc\_b}^{p}\times\mathrm{d}\mathbf{F}_{xc\_b}^{p}\end{cases}. \tag{9}$$

The vector of force and moment acting on contact point of raceway is shown as

$$\begin{cases}\mathrm{d}\,\mathbf{F}_{xc\_r}^{p}=-\mathrm{d}\,\mathbf{F}_{xc\_b}^{p}\\ \mathrm{d}\,\mathbf{M}_{xc\_r}^{p}=\left(T_{a\_p}T_{i\_a}^{-1}\mathbf{r}_{xc\_r}^{i}\right)\times\mathrm{d}\,\mathbf{F}_{xc\_r}^{p}\end{cases}. \tag{10}$$

The force and torque vector of raceway acting on the ball are obtained by the integration around every contact strips

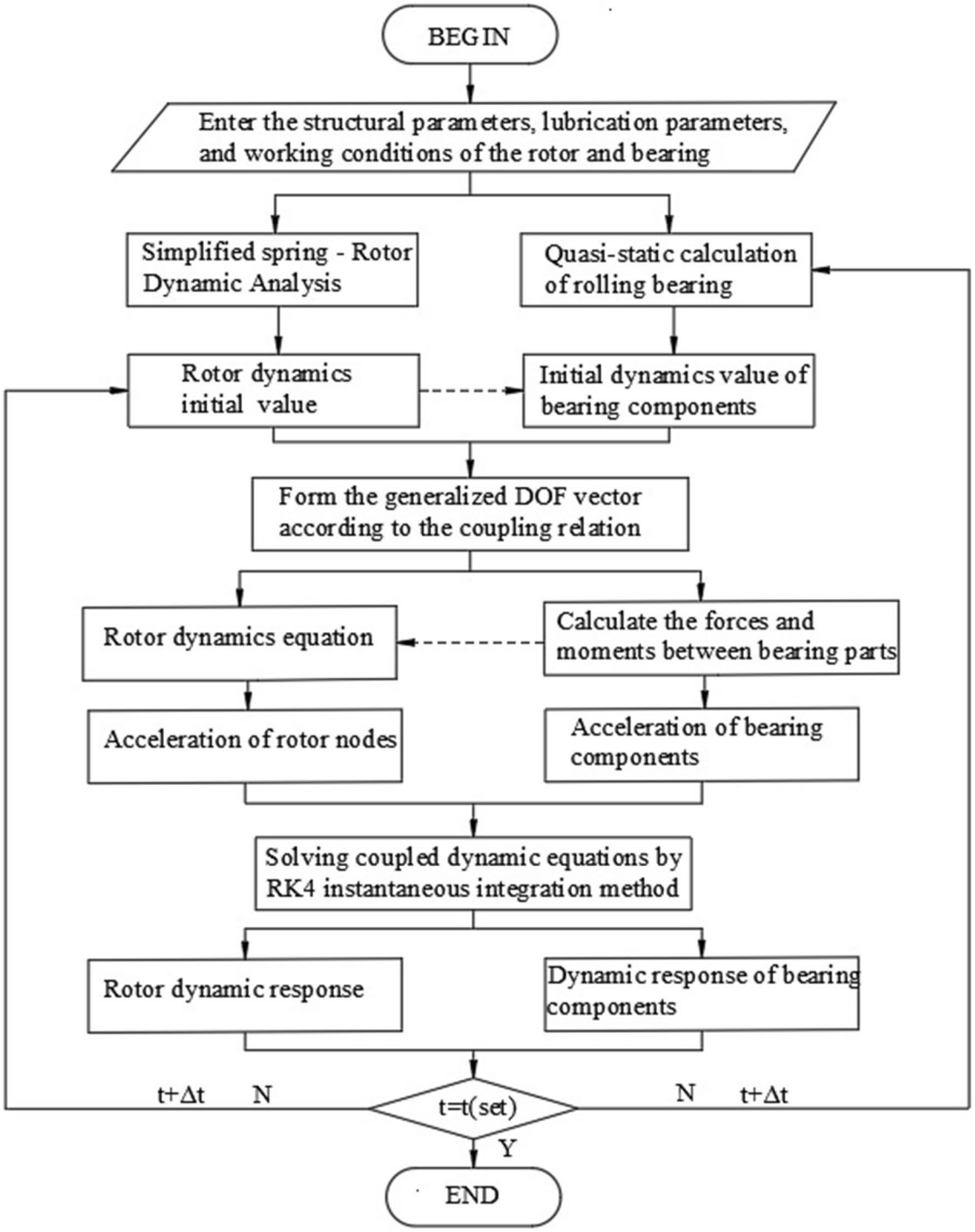

Fig. 8 The process to solve coupled dynamic equations

$$\begin{cases} \mathbf{F}^{\mathrm{a}}_{\mathrm{b\_r}} = T^{-1}_{\mathrm{a\_p}}\left(\int \mathrm{d}\,\mathbf{F}^{\mathrm{p}}_{\mathrm{xc\_b}}\right) \\ \mathbf{M}^{\mathrm{a}}_{\mathrm{b\_r}} = T^{-1}_{\mathrm{a\_p}}\left(\int \mathrm{d}\,\mathbf{M}^{\mathrm{p}}_{\mathrm{xc\_b}}\right) \end{cases}. \tag{11}$$

The force and torque vector of ball acting on the ring are obtained as

$$\begin{cases} \mathbf{F}^{\mathrm{i}}_{\mathrm{b\_r}} = \sum_{i=1}^{n_{\mathrm{b}}}\left(T^{-1}_{\mathrm{i\_a}}T^{-1}_{\mathrm{a\_p}}\left(\int \mathrm{d}\,\mathbf{F}^{\mathrm{p}}_{\mathrm{xc\_r}}\right)\right) \\ \mathbf{M}^{\mathrm{r}}_{\mathrm{b\_r}} = \sum_{i=1}^{n_{\mathrm{b}}}\left(T_{\mathrm{i\_r}}T^{-1}_{\mathrm{i\_a}}T^{-1}_{\mathrm{a\_c}}\left(\int \mathrm{d}\,\mathbf{M}^{\mathrm{p}}_{\mathrm{xc\_r}}\right)\right) \end{cases}, \tag{12}$$

where n_{b} is the number of balls.

Table 1 System parameters of ball bearing–rotor system

Item	Parameter	Value
Ball bearing	Number of balls	9
	Contact angle	25°
	Pitch diameter	20.45 mm
	Ball diameter	4.74 mm
	Inner race clearance	0.001 mm
	Outer race clearance	0.002 mm
	Inner diameter of cage	21 mm
	Outer diameter of cage	17 mm
	Pocket clearance	0.2 mm
Rotor	*L*	177.5 mm
	D	10 mm
	Outer diameter	72 mm
	Length of disk	25.7 mm
	Rotor density	7950 kg m^{-3}
	Modulus of elasticity	211 GPa
	Disk eccentricity	32 μm

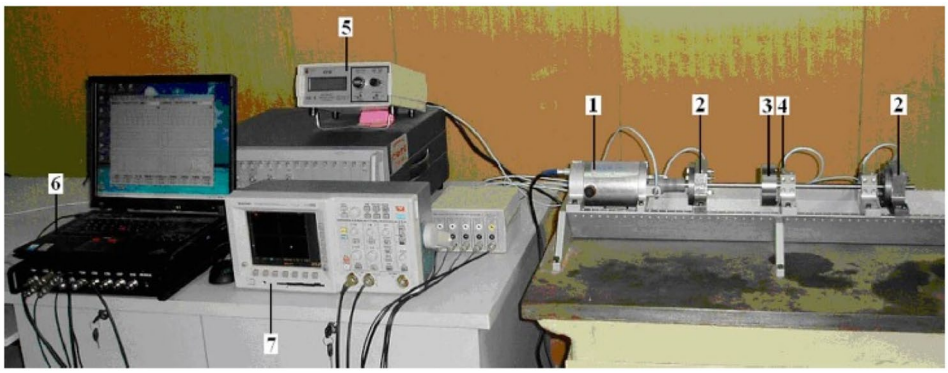

(a)

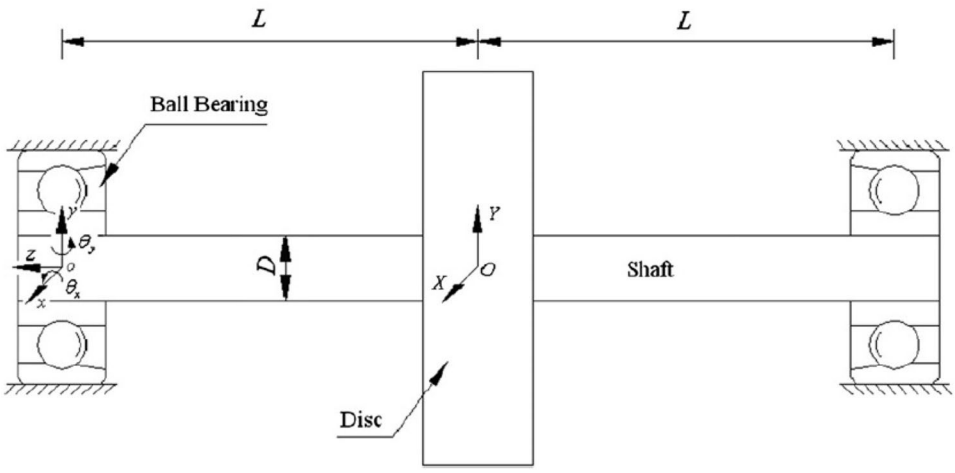

(b)

Fig. 9 Ball bearing–rotor system test rig and the corresponding structure in the reference [22]. **a** Test rig and **b** structure of ball bearing–rotor system

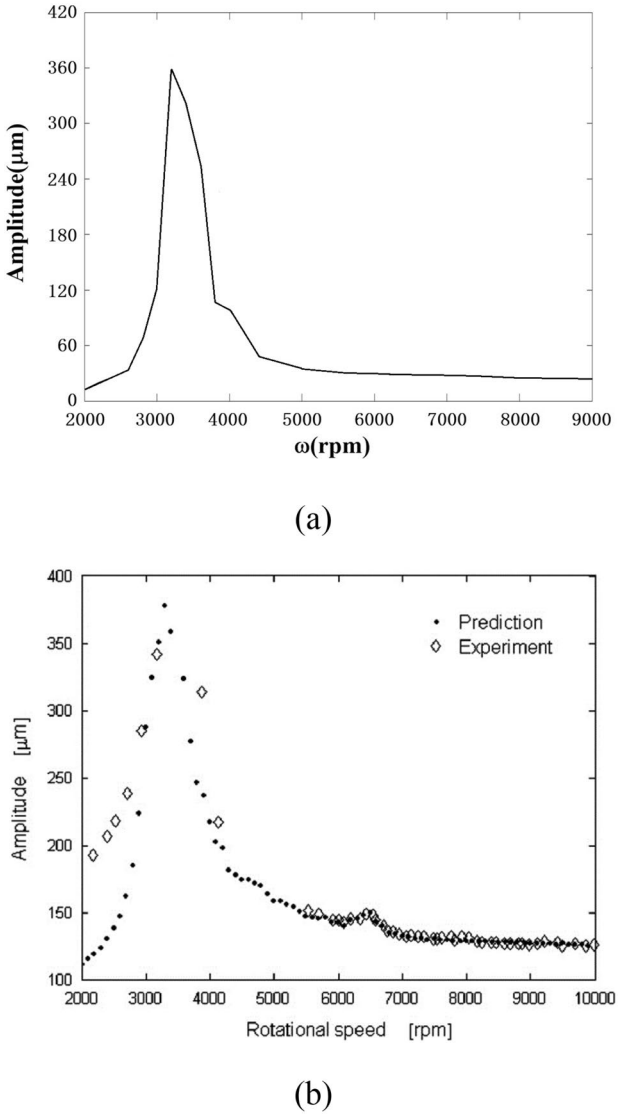

Fig. 10 The vibration diagram of disk from this paper and the reference [22]. **a** Vibration diagram from this paper and **b** vibration diagram from the reference [22]

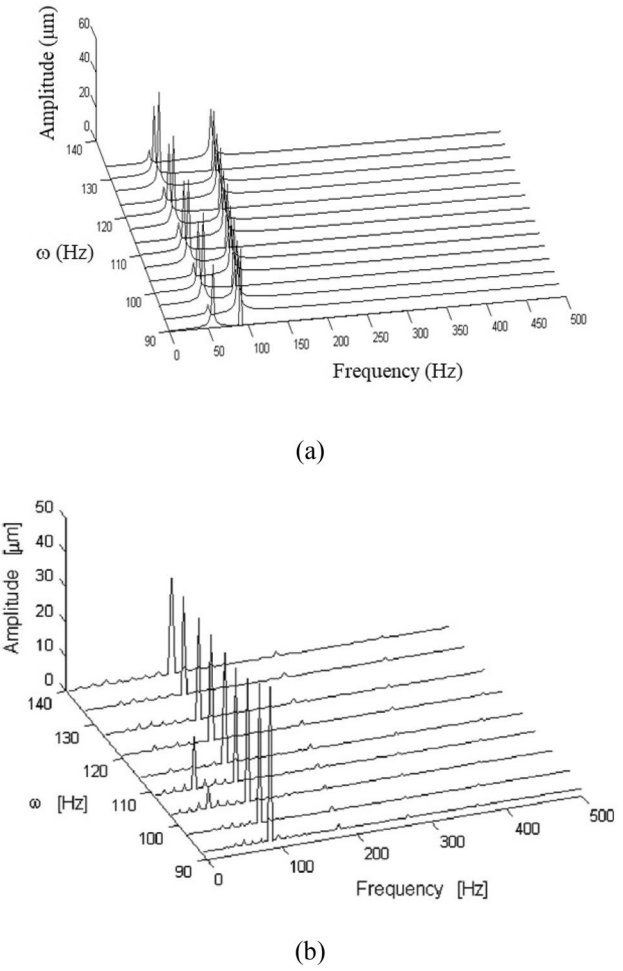

Fig. 11 The vibration waterfall diagram of disk vibration during the speed range from 5400 to 8400 rpm and **a** waterfall diagram in this paper and **b** waterfall diagram from the reference [22]

Interactive Force Between Ball and Cage

The relative geometric position between the ball and cage pocket is shown in Fig. 4. In the pocket coordinate system, the position vector of the ball center relative to pocket center is expressed as

$$\mathbf{r}_{\mathrm{b\_d}}^{\mathrm{d}} = T_{\mathrm{c\_d}}\left(T_{\mathrm{i\_c}}\mathbf{r}_{\mathrm{b\_c}}^{\mathrm{i}} - \mathbf{r}_{\mathrm{d\_c}}^{\mathrm{c}}\right). \tag{13}$$

Then, the minimum clearance between ball and pocket wall is shown as

$$h_{\mathrm{bd}} = 0.5B_{\mathrm{d}} - \sqrt{\left(r_{\mathrm{b\_d1}}^{\mathrm{d}}\right)^2 + \left(r_{\mathrm{b\_d2}}^{\mathrm{d}}\right)^2}, \tag{14}$$

where B_{d} is the width of pocket.

In the contact (between ball and pocket) coordinate system, the position vector of cage center is

$$\begin{cases} \mathbf{r}_{\mathrm{p\_b}}^{\mathrm{p}} = \left(\begin{array}{ccc} 0 & 0.5d_{\mathrm{b}} & 0 \end{array}\right)^T \\ \mathbf{r}_{\mathrm{p\_c}}^{\mathrm{p}} = \mathbf{r}_{\mathrm{p\_b}}^{\mathrm{p}} + T_{\mathrm{d\_p}}\mathbf{r}_{\mathrm{b\_d}}^{\mathrm{d}} + T_{\mathrm{d\_p}}T_{\mathrm{c\_d}}\mathbf{r}_{\mathrm{d\_c}}^{\mathrm{c}} \end{cases}. \tag{15}$$

The relative velocity vector between ball and cage is

$$\begin{aligned} \mathbf{v}_{\mathrm{b\_c}}^{\mathrm{p}} = {} & T_{\mathrm{d\_p}}T_{\mathrm{c\_d}}T_{\mathrm{i\_c}}\mathbf{v}_{\mathrm{c}}^{\mathrm{i}} + \left(T_{\mathrm{d\_p}}T_{\mathrm{c\_d}}\boldsymbol{\omega}_{\mathrm{c}}^{\mathrm{c}}\right) \times \mathbf{r}_{\mathrm{p\_c}}^{\mathrm{p}} \\ & - \left(T_{\mathrm{d\_p}}T_{\mathrm{c\_d}}T_{\mathrm{i\_c}}\mathbf{v}_{\mathrm{b}}^{\mathrm{i}} + \left(T_{\mathrm{d\_p}}T_{\mathrm{c\_d}}T_{\mathrm{i\_c}}T_{\mathrm{i\_b}}^{-1}\boldsymbol{\omega}_{\mathrm{b}}^{\mathrm{b}}\right) \times \mathbf{r}_{\mathrm{p\_b}}^{\mathrm{p}}\right). \end{aligned} \tag{16}$$

Taking the comprehensive roughness σ_{bd} between the ball and pocket surface as a reference, when $h_{\mathrm{bd}} \geq \sigma_{\mathrm{bd}}$, there is

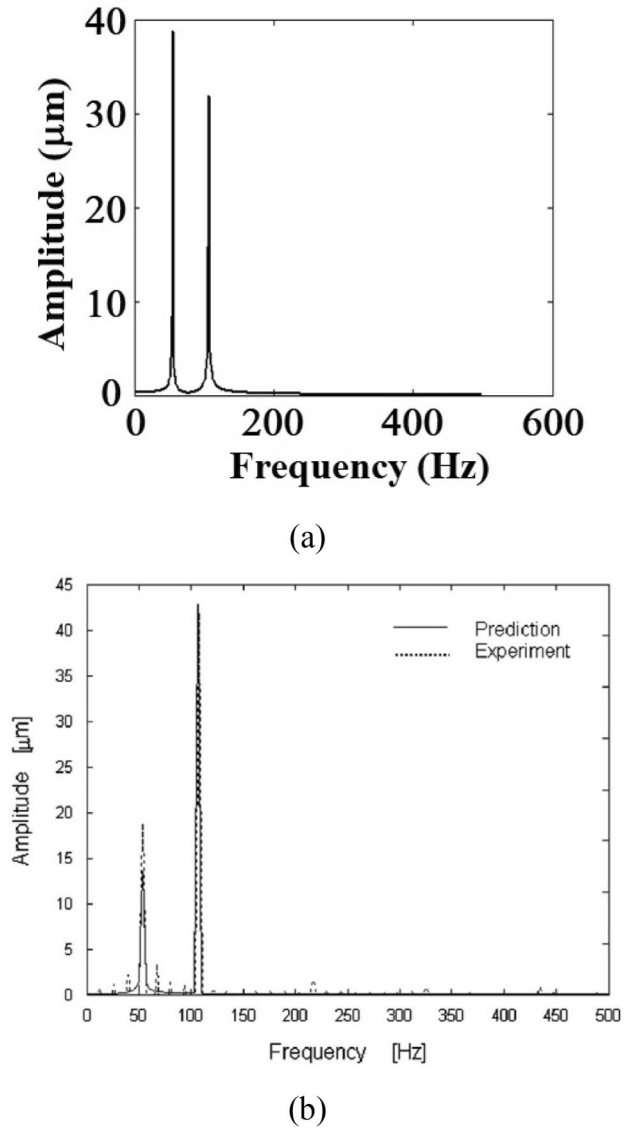

Fig. 12 The vibration diagram of disk at 6400 rpm from this paper and the reference [22]. **a** Vibration diagram from this paper and **b** vibration diagram from the reference [22]

hydrodynamic pressure between the ball and cage pocket and the contact force is calculated by Brewe formula [20].

When $h_{bd} < \sigma_{bd}$, the contact force is obtained according to the contact deformation between ball and pocket.

$$\begin{cases} F_{bd} = K_{bd}\left(\sigma_{bd} - h_{bd}\right)^{1.5} - c_n v^p_{b\_c2}, \\ F_{\mu} = \mu_{bc}\left|F_{bd}\right| \end{cases} \tag{17}$$

where K_{bd} is Hertz contact stiffness; c_n is contact damping; μ_{bc} is traction coefficient; F_μ is traction force.

The force and torque vector of cage acting on the ball are obtained

Table 2 The variables of structure, material and lubrication about the asymmetric system

Item	Variables	Value	
		Left bearing	Right bearing
Bearing	Diameter of pitch circle	65.004 mm	70.004 mm
	Bearing width	20 mm	20 mm
	The number of balls	12	15
	Initial contact angle	15°	15°
	The ball diameter	12.3 mm	12.3 mm
	Width of cage	17 mm	17 mm
	Inner diameter of cage	61 mm	66 mm
	Outer diameter of cage	72 mm	77 mm
	Guide clearance of cage	0.4 mm	0.4 mm
	Pocket clearance	0.2 mm	0.2 mm
Rotor	Rotor diameter	50 mm	
	Rotor length	500 mm	
	Outer diameter of disk	100 mm	
	Disk thickness	60 mm	
	Bearing span	400 mm	
	Mass eccentricity	5 μm	
Material	Elastic modulus	208 GPa	
	Poisson's ratio	0.30	
	Density of ball, ring and rotor	7800 kg·m^{-3}	
	Density of cage	1250 kg·m^{-3}	
Oil	Operating temperature	25°	
	Oil lubrication density	980 kg·m^{-3}	
	Dynamic viscosity of oil	0.033 Pa·s	
	Coefficient of viscosity	1.28×10^{-8} Pa^{-1}	

$$\begin{cases} \mathbf{F}^a_{c\_b} = T_{i\_a}T^{-1}_{i\_c}T^{-1}_{c\_d}T^{-1}_{d\_p}\mathbf{F}_v \\ \mathbf{M}^a_{c\_b} = T_{i\_a}T^{-1}_{i\_c}T^{-1}_{c\_d}T^{-1}_{d\_p}\mathbf{r}^p_{p\_b}\times\mathbf{F}_v \end{cases}, \tag{18}$$

with $\varphi_v = \arctan(-v^p_{b\_c1}/v^p_{b\_c3})$ being the angle between relative velocity vector and Z_p axis; $\mathbf{F}_v = (F_\mu \sin\varphi_v, -F_{bd}, F_\mu\cos\varphi_v)$.

The force and torque vector of ball acting on the cage are shown as

$$\begin{cases} \mathbf{F}^i_{b\_c} = \sum_{i=1}^{n_b}\left(-T^{-1}_{i\_c}T^{-1}_{c\_d}T^{-1}_{d\_p}\mathbf{F}_v\right) \\ \mathbf{M}^c_{b\_c} = \sum_{i=1}^{n_b}\left(-T^{-1}_{c\_d}T^{-1}_{d\_p}\mathbf{r}^p_{p\_c}\times\mathbf{F}_v\right) \end{cases}. \tag{19}$$

Interactive Force Between Ring and Cage

Figure 5 describes the relative geometric position between outer ring and cage. In general, the cage is guided by outer

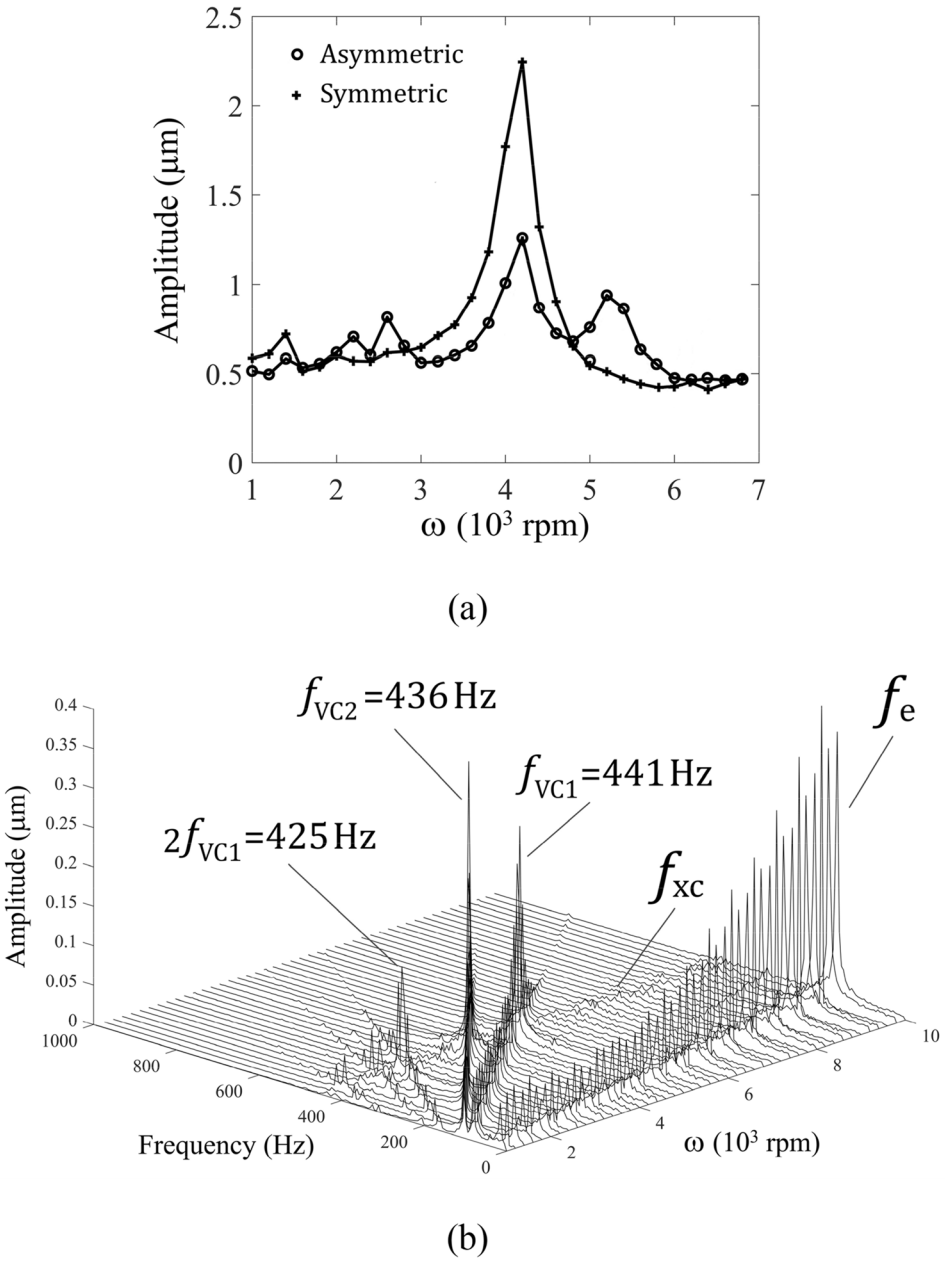

Fig. 13 The vibration diagram and waterfall spectrum of disk for both symmetric and asymmetric support. **a** Vibration diagram and **b** waterfall spectrum

ring for high-speed ball bearing. Therefore, this section only analyzes the interaction between cage and outer ring, but the analysis process is also applicable to bearing guided by inner ring.

It is assumed that P_c is the closest point on the cage to the surface of outer ring, and P_r is the corresponding point on the outer ring. If there is no contact between cage and outer ring (P_c and P_r do not coincide), the hydrodynamic effect between the two parts can be calculated according to the short sliding bearing theory [20].

If there is contact between the outer ring and cage, P_c and P_r will meet together and the coincidence point is recorded as P. In the body-fixed coordinate system of cage, the position vector from point P_c to cage center is written as

$$\mathbf{r}_{p\_c}^{c} = \left(\frac{B_c}{2} \ -\frac{D_c}{2}\sin\theta_c \ \frac{D_c}{2}\cos\theta_c \right)^T, \tag{20}$$

where B_c and D_c are the width and diameter of cage guide surface; θ_c is the azimuth angle of point P_c in the body-fixed coordinate system of cage.

In the body-fixed coordinate system of outer ring, the position vector from point P_r to ring center is expressed as

$$\mathbf{r}_{p\_r}^{r} = T_{i\_r}\left(\mathbf{r}_c^i - \mathbf{r}_r^i\right) + T_{i\_r}T_{i\_c}^{-1}\mathbf{r}_{p\_c}^{c}. \tag{21}$$

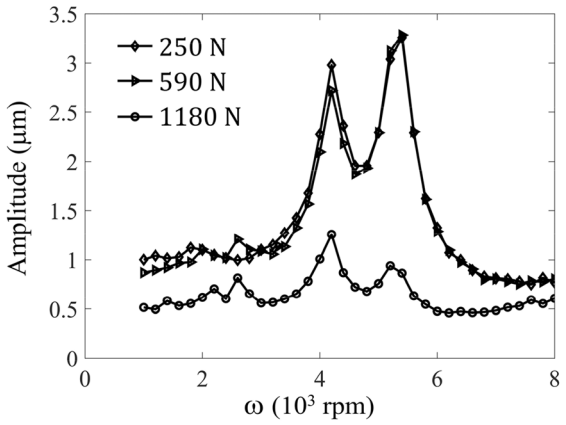

(a)

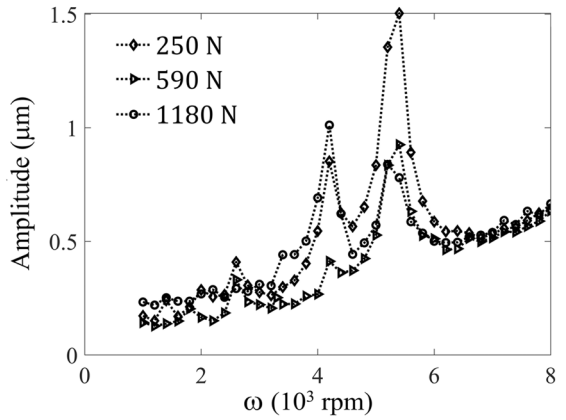

(b)

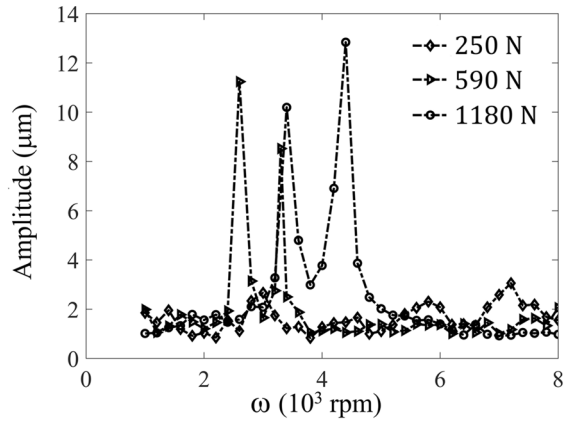

(c)

Fig. 14 The vibration diagram of rotor disk under asymmetric support in 3 directions. **a** Horizontal vibration, **b** vertical vibration and **c** axial vibration

It is supposed that the contact area of cage is divided into several n narrow strips, the position vector from k-th strip to cage center is obtained as

$$\mathbf{r}_{\mathrm{p\_k}}^{\mathrm{c}}=\left(B_{\mathrm{c}}-\frac{(k-0.5)B_{\mathrm{c}}}{n},-\frac{D_{\mathrm{c}}}{2}\sin\theta_{\mathrm{c}},\frac{D_{\mathrm{c}}}{2}\cos\theta_{\mathrm{c}}\right)^{T}. \tag{22}$$

In the contact coordinate system between cage and outer ring, the relative sliding velocity between k-th strip on cage guide surface and ring guide surface is written as

$$\begin{aligned} v_{\mathrm{c\_r}}^{\mathrm{p}} &= T_{\mathrm{r\_p}}T_{\mathrm{i\_r}}v_{\mathrm{r}}^{\mathrm{i}}+T_{\mathrm{r\_p}}\left(\boldsymbol{\omega}_{\mathrm{r}}^{\mathrm{r}}\times\mathbf{r}_{\mathrm{p\_r}}^{\mathrm{r}}\right)\\ &\quad-\left[T_{\mathrm{r\_p}}T_{\mathrm{i\_r}}v_{\mathrm{c}}^{\mathrm{i}}+T_{\mathrm{r\_p}}T_{\mathrm{i\_r}}T_{\mathrm{i\_c}}^{-1}\left(\boldsymbol{\omega}_{\mathrm{c}}^{\mathrm{c}}\times\mathbf{r}_{\mathrm{p\_k}}^{\mathrm{c}}\right)\right]. \end{aligned} \tag{23}$$

In the body-fixed coordinate system of outer ring, the position vector from k-th strip on the cage contact area to outer ring center is as the following formula

$$\mathbf{r}_{\mathrm{p\_r}}^{\mathrm{r}}=T_{\mathrm{i\_r}}\mathbf{r}_{\mathrm{c\_r}}^{\mathrm{i}}+T_{\mathrm{i\_r}}T_{\mathrm{i\_c}}^{-1}\mathbf{r}_{\mathrm{p\_k}}^{\mathrm{c}}. \tag{24}$$

Then, the minimum clearance between k-th strip on the cage guide surface and outer ring guide surface is shown as

$$C_{\mathrm{crk}}=\left(\frac{D_{\mathrm{c}}}{2}-\sqrt{\left(\mathbf{r}_{\mathrm{p\_r2}}^{\mathrm{r}}\right)^{2}+\left(\mathbf{r}_{\mathrm{p\_r3}}^{\mathrm{r}}\right)^{2}}\right). \tag{25}$$

Therefore, the discriminant to judge whether the contact between cage and ring appears is shown as

$$\delta_{\mathrm{cr}}=R_{\mathrm{cr}}-C_{\mathrm{crk}}, \tag{26}$$

with R_{cr} being the radius of guide surface of the cage or ring.

When $\delta_{\mathrm{cr}}\le 0$, k-th strip on the cage has no contact with the outer ring. Meanwhile, the fluid lubrication force on the k-th strip can be calculated according to short sliding bearing theory.

When $\delta_{\mathrm{cr}}>0$, it shows that k-th strip on the cage contacts with the outer ring. The normal and tangential force can be obtained using the line contact formula.

$$\begin{cases} F_{\mathrm{ck\_n}}=K_{\mathrm{k}}\left(\delta_{\mathrm{cr}}\right)^{\frac{10}{9}}\\ F_{\mathrm{ck\_f}}=\mu_{\mathrm{cr}}F_{\mathrm{ck\_n}} \end{cases}, \tag{27}$$

where K_{k} stands for the Hertz contact coefficient of k-th strip; μ_{cr} is boundary friction factor.

Then, the force and torque vector of outer ring acting on the k-th strip of cage guide surface is shown as

$$\begin{cases} \mathbf{F}_{\mathrm{r\_ck}}^{\mathrm{p}}=\left(F_{\mathrm{ck\_f}}\sin\theta_{\mathrm{cr}}\;\;F_{\mathrm{ck\_f}}\cos\theta_{\mathrm{cr}}\;\;F_{\mathrm{ck\_n}}\right)^{T}\\ \mathbf{M}_{\mathrm{r\_ck}}^{\mathrm{p}}=\mathbf{r}_{\mathrm{r\_ck}}^{\mathrm{p}}\times\mathbf{F}_{\mathrm{r\_ck}}^{\mathrm{p}} \end{cases}. \tag{28}$$

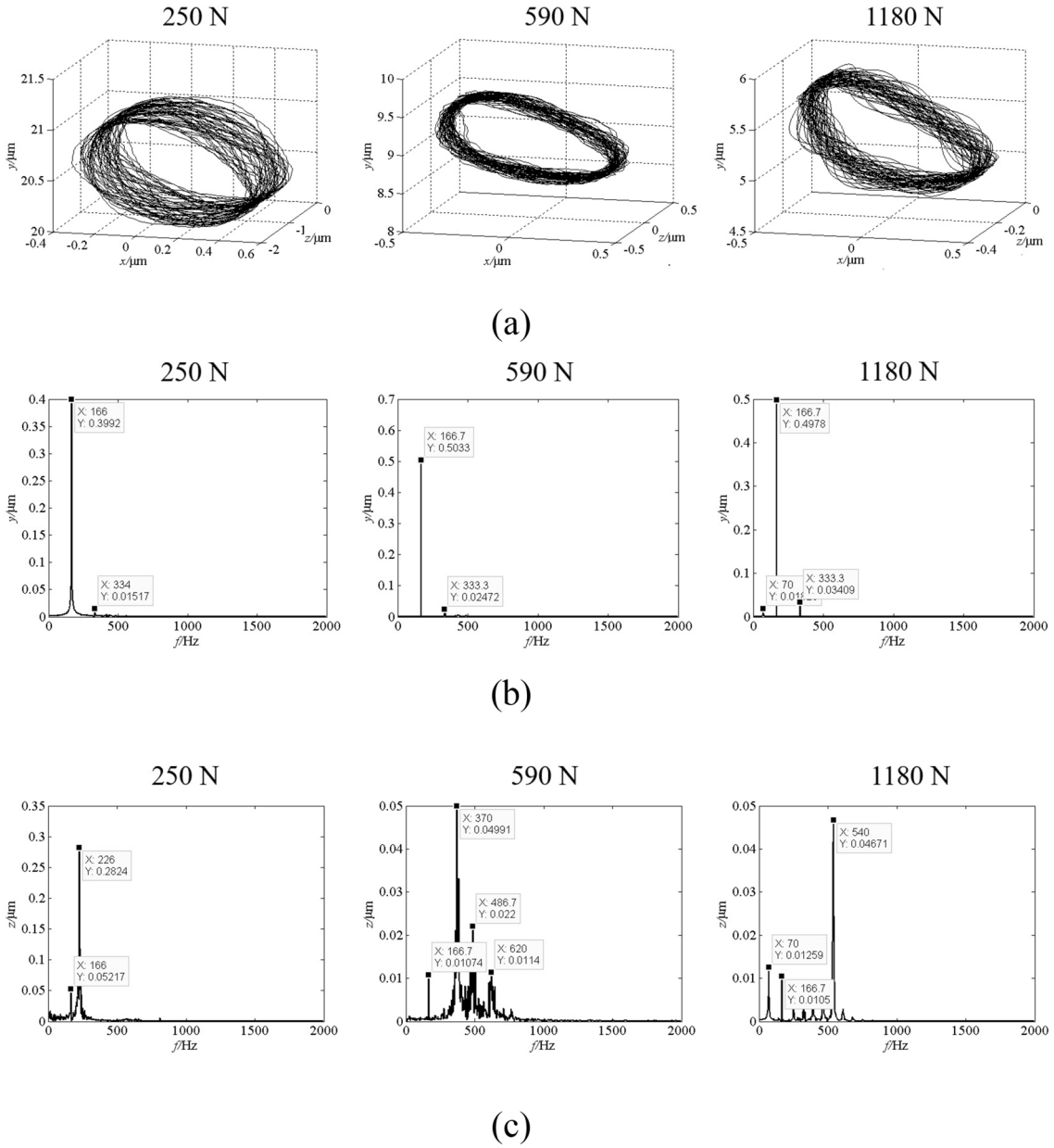

Fig. 15 The dynamic characteristics of rotor disk under different preload forces. **a** Axial displacement of ball, **b** frequency components in the vertical direction and **c** frequency components in the axial direction

In the body-fixed coordinate system of cage, the total force and moment of the outer ring guide surface on the cage guide surface are written as

$$\begin{cases} \mathbf{F}_{\mathrm{r\_c}}^{\mathrm{i}} = \sum_{k=1}^{m} \left(T_{\mathrm{r\_i}} T_{\mathrm{p\_r}} \mathbf{F}_{\mathrm{r\_ck}}^{\mathrm{p}} \right) \\ \mathbf{M}_{\mathrm{r\_c}}^{\mathrm{i}} = \sum_{k=1}^{m} \left(T_{\mathrm{r\_i}} \mathbf{r}_{\mathrm{p\_r}}^{\mathrm{r}} \times T_{\mathrm{i\_r}} \mathbf{F}_{\mathrm{r\_ck}}^{\mathrm{i}} \right) \end{cases}. \tag{29}$$

Dynamic Equations of Ball Bearing

According to Newton–Euler motion theory, the corresponding translational and rotational equations of mass center can be established for each part.

In the inertial Cartesian coordinate system, the translational equations of ring and cage are shown as

$$\begin{cases} m_{\mathrm{r}}\ddot{x}_{\mathrm{r}} = F_{\mathrm{rx}}, m_{\mathrm{r}}\ddot{y}_{\mathrm{r}} = F_{\mathrm{ry}}, m_{\mathrm{r}}\ddot{z}_{\mathrm{r}} = F_{\mathrm{rz}} \\ m_{\mathrm{c}}\ddot{x}_{\mathrm{c}} = F_{\mathrm{cx}}, m_{\mathrm{c}}\ddot{y}_{\mathrm{c}} = F_{\mathrm{cy}}, m_{\mathrm{c}}\ddot{z}_{\mathrm{c}} = F_{\mathrm{cz}} \end{cases}. \tag{30}$$

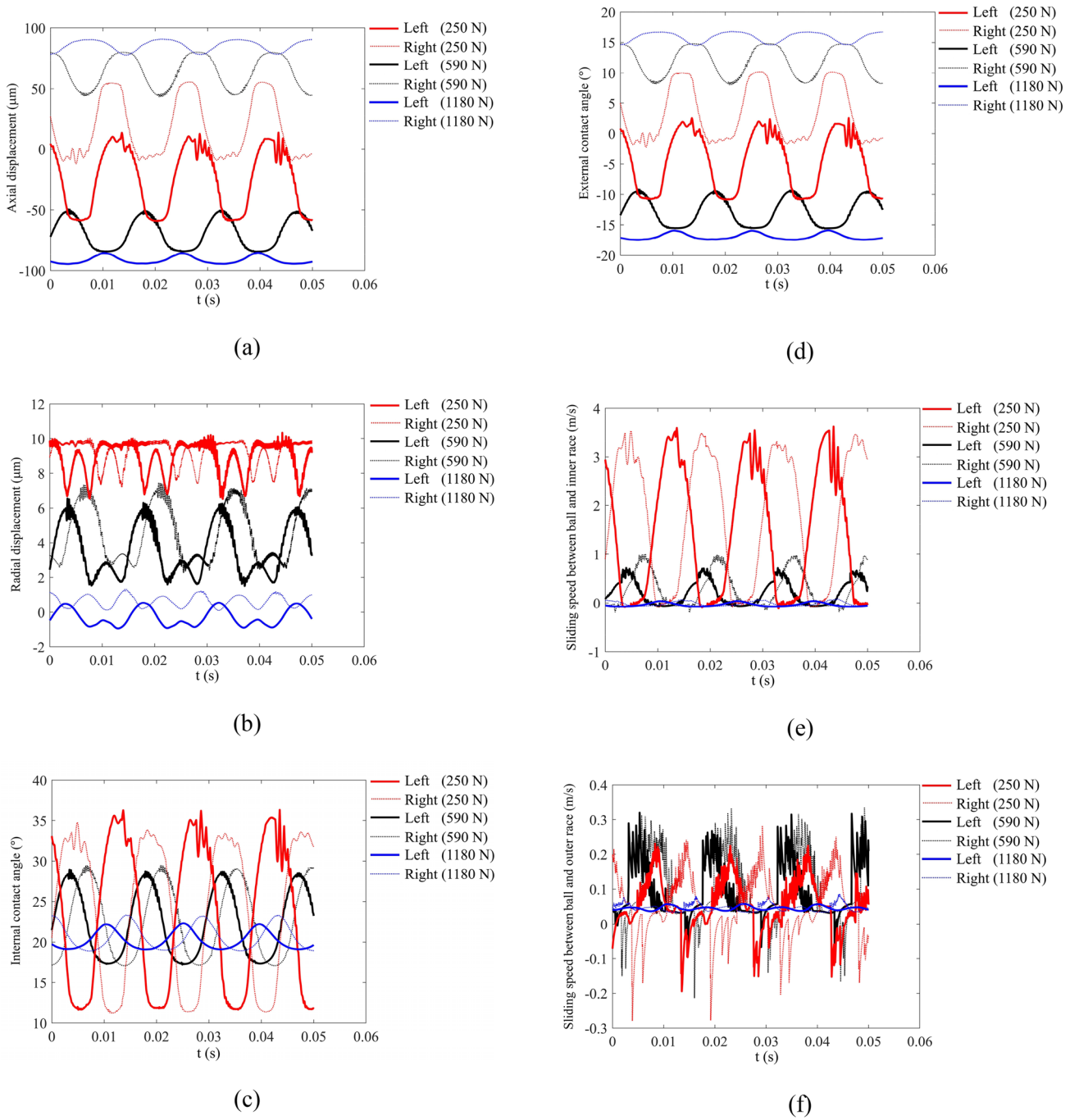

Fig. 16 The dynamic features of ball for the asymmetric bearings. **a** Axial displacements, **b** radial displacement, **c** internal contact angle, **d** external contact angle, **e** sliding speed between ball and inner race and **f** sliding speed between ball and outer race

In the inertial cylindrical coordinate system, the translation equations of balls are described as follows:

$$\begin{cases} m_{\mathrm{b}}\ddot{x}_{\mathrm{b}} = F_{\mathrm{bx}} \\ m_{\mathrm{b}}\ddot{r}_{\mathrm{b}} - m_{\mathrm{b}}r_{\mathrm{b}}\dot{\theta}_{\mathrm{b}}^2 = F_{\mathrm{br}} \\ m_{\mathrm{b}}r_{\mathrm{b}}\ddot{\theta}_{\mathrm{b}} + 2m_{\mathrm{b}}\dot{r}_{\mathrm{b}}\dot{\theta}_{\mathrm{b}} = F_{\mathrm{b}\theta} \end{cases}. \tag{31}$$

In the body-fixed coordinate systems, the rotational equations of ring are unified.

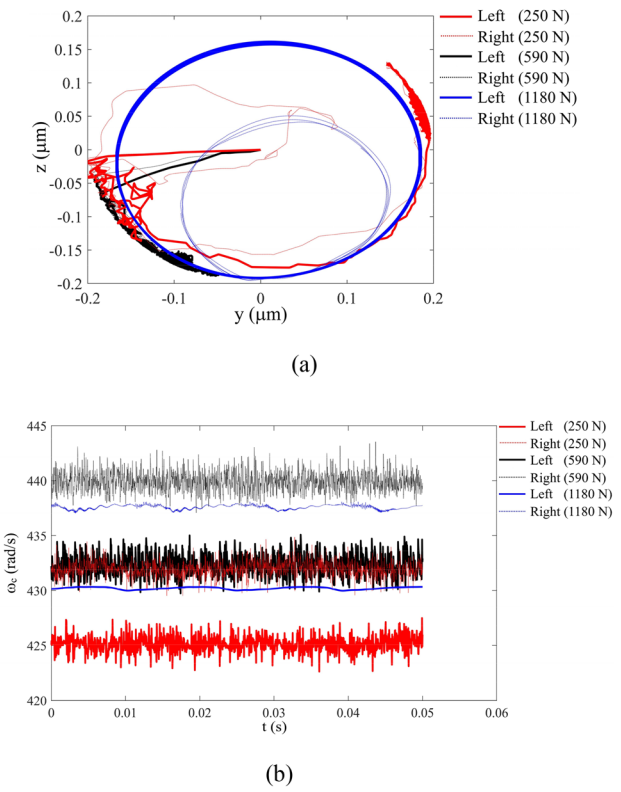

Fig. 17 The dynamic features of cage for the asymmetric bearings. **a** Orbits of mass center and **b** the speed fluctuation diagram of cage

$$\begin{cases} I_{rx}\dot{\omega}_{rx} - \left(I_{ry} - I_{rz}\right)\omega_{ry}\omega_{rz} = M_{rx} \\ I_{ry}\dot{\omega}_{ry} - \left(I_{rz} - I_{rx}\right)\omega_{rz}\omega_{rx} = M_{ry} \\ I_{rz}\dot{\omega}_{rz} - \left(I_{rx} - I_{ry}\right)\omega_{rx}\omega_{ry} = M_{rz} \end{cases}. \tag{32}$$

with I standing for moment of inertia; the equations of ball and cage can also use Eq. (32) to analyze the dynamic behavior of ball bearings.

Dynamic Model of Elastic Rotor

The rotor in Fig. 1 is composed of a shaft and a disk. The shaft is discretized by several Timoshenko beam element (Fig. 6) which considers the moment of inertia, shear effect and axial force effect [21]. This element includes 3 translation DOFs (x, y, z) and 2 rotational DOFs (ψ, φ). Each element matrix is assembled according to the relative geometric position to form an integral matrix of the shaft.

The disk is treated as a rigid disk which is simplified as lumped parameter element and incorporated into the shaft segment matrix according to Hamilton principle. Finally, the equations of rotor are formed.

$$\left(\mathbf{M}_S + \mathbf{M}_D\right)\ddot{\mathbf{u}}_R + \left(\mathbf{G}_S + \mathbf{G}_D\right)\dot{\mathbf{u}}_R + \mathbf{K}_s\mathbf{u}_R = \mathbf{F}_B + \mathbf{F}_U + \mathbf{F}_G, \tag{33}$$

where $\mathbf{M}_S$, $\mathbf{G}_S$ and $\mathbf{K}_S$ are the mass, gyroscopic moment and stiffness matrix of shaft segments; $\mathbf{M}_D$ and $\mathbf{G}_D$ are the mass and gyroscopic moment matrix of rigid disk; the vectors of bearing force $\mathbf{F}_B$ can be expressed as $\mathbf{F}_B = (0,\ldots, F_{Bx\_1}, F_{By\_1}, F_{Bz\_1}, M_{B\psi\_1}, F_{B\varphi\_1},\ldots, F_{Bx\_1}, F_{By\_1}, F_{Bz\_1}, M_{B\psi\_1}, F_{B\varphi\_1},\ldots,0)^T$ with subscripts '1' and '2' meaning the first and second ball bearing; $\mathbf{F}_Q$ and $\mathbf{F}_G$ are the vectors of unbalance force and gravity; $\mathbf{u}_R$ is the displacement vector of rotor; n_s is the number of nodes for the shaft.

Coupled Dynamics Model of Asymmetric Ball Bearing–Rotor System

Figure 7 shows the coupled dynamic model of ball bearing–rotor system. The rotor in Fig. 1 has been divided into (n_s-1) elements and n_s node. Under normal conditions, the mass of ring is much smaller than that of rotor; as a result, the motion of inner ring is determined by the journal position of rotor which is controlled by rotor dynamic equations; at the same time, the force and torque from other bearing parts (balls and cage) acting on the inner ring are transferred to the corresponding journal position to provide supporting force and moment which are determined by the dynamic equations of ball bearings.

According to the above coordination relationship, the following motion constraint equation can be established after transforming the DOFs of rotor in the bearing coordinate system.

$$\begin{cases} \mathbf{u}_{Bi} = (x_{Bi}, y_{Bi}, z_{Bi}, \dot{x}_{Bi}, \dot{y}_{Bi}, \dot{z}_{Bi}, \eta_{Bi}, \xi_{Bi}, \lambda_{Bi}, \dot{\eta}_{Bi}, \dot{\xi}_{Bi}, \dot{\lambda}_{Bi})^T \\ \mathbf{u}_{Rj} = (z_{Rj}, -x_{Rj}, -y_{Rj}, \dot{z}_{Rj}, -\dot{x}_{Rj}, -\dot{y}_{Rj}, \omega_R t, -\psi_{Rj}, -\varphi_{Rj}, \omega_R, -\dot{\psi}_{Rj}, -\dot{\varphi}_{Rj})^T \\ \mathbf{u}_{Bi} = \mathbf{u}_{Rj} \quad (i = 1, 2; j = 1, \ldots, n_s) \end{cases}, \tag{34}$$

where $\mathbf{u}_{Bi}$ is the combined translation and rotation vector of ith bearing; $\mathbf{u}_{Rj}$ is the combined translation and rotation vector of jth node on the rotor corresponding to the position of ith bearing; ω_R is the angular velocity of rotor; t is time.

Similarly, the force and torque constraint equations can be built in the rotor coordinate system.

$$\begin{cases} \mathbf{F}_{\mathrm{Bi}} = \left(-F_{\mathrm{Bi\_y}}, -F_{\mathrm{Bi\_z}}, -F_{\mathrm{Bi\_x}}, -M_{\mathrm{Bi\_y}}, -M_{\mathrm{Bi\_z}}, 0\right)^T \\ \mathbf{F}_{\mathrm{Rj}} = \left(F_{\mathrm{Rj\_x}}, F_{\mathrm{Rj\_y}}, F_{\mathrm{Rj\_z}}, M_{\mathrm{Rj\_x}}, M_{\mathrm{Rj\_y}}, 0\right)^T \\ \mathbf{F}_{\mathrm{Rj}} = \mathbf{F}_{\mathrm{Bi}} \quad (i = 1, 2; \quad j = 1, \ldots, n_{\mathrm{s}}) \end{cases} . \tag{35}$$

Therefore, the coupled dynamics model of angular-contact ball bearing–rotor system can be obtained by combining bearing dynamic equations (formula 30–32), rotor dynamic equations (formula 33) and constraint equations (formula 34–35).

As a result, the generalized vector $\mathbf{q}$ of bearing–rotor system which includes displacement vector and velocity vector can be established.

$$\begin{cases} \mathbf{q} = (\mathbf{u}_{\mathrm{R}}, \mathbf{u}_{\mathrm{B1}}, \mathbf{u}_{\mathrm{B2}}, \dot{\mathbf{u}}_{\mathrm{R}}, \dot{\mathbf{u}}_{\mathrm{B1}}, \dot{\mathbf{u}}_{\mathrm{B2}})^T \\ \mathbf{u}_{\mathrm{R}} = (x_{\mathrm{R\_1}}, y_{\mathrm{R\_1}}, z_{\mathrm{R\_1}}, \psi_{\mathrm{R\_1}}, \varphi_{\mathrm{R\_1}}, \cdots, \\ x_{\mathrm{R\_n_s}}, y_{\mathrm{R\_n_s}}, z_{\mathrm{R\_n_s}}, \psi_{\mathrm{R\_n_s}}, \varphi_{\mathrm{R\_n_s}})^T \\ \mathbf{u}_{\mathrm{B1}} = (x_{\mathrm{r1}}, y_{\mathrm{r1}}, z_{\mathrm{r1}}, \eta_{\mathrm{r1}}, \xi_{\mathrm{r1}}, \lambda_{\mathrm{r1}}, \\ x_{\mathrm{c1}}, y_{\mathrm{c1}}, z_{\mathrm{c1}}, \eta_{\mathrm{c1}}, \xi_{\mathrm{c1}}, \lambda_{\mathrm{c1}}, \\ x_{\mathrm{b1\_1}}, r_{\mathrm{b1\_1}}, \theta_{\mathrm{b1\_1}}, \eta_{\mathrm{b1\_1}}, \xi_{\mathrm{b1\_1}}, \lambda_{\mathrm{b1\_1}}, \cdots, \\ x_{\mathrm{b1\_n_b}}, r_{\mathrm{b1\_n_b}}, \theta_{\mathrm{b1\_n_b}}, \eta_{\mathrm{b1\_n_b}}, \xi_{\mathrm{b1\_n_b}}, \lambda_{\mathrm{b1\_n_b}})^T \\ \mathbf{u}_{\mathrm{B2}} = (x_{\mathrm{r2}}, y_{\mathrm{r2}}, z_{\mathrm{r2}}, \eta_{\mathrm{r2}}, \xi_{\mathrm{r2}}, \lambda_{\mathrm{r2}}, \\ x_{\mathrm{c2}}, y_{\mathrm{c2}}, z_{\mathrm{c2}}, \eta_{\mathrm{c2}}, \xi_{\mathrm{c2}}, \lambda_{\mathrm{c2}}, \\ x_{\mathrm{b2\_1}}, r_{\mathrm{b2\_1}}, \theta_{\mathrm{b2\_1}}, \eta_{\mathrm{b2\_1}}, \xi_{\mathrm{b2\_1}}, \lambda_{\mathrm{b2\_1}}, \cdots, \\ x_{\mathrm{b2\_n_b}}, r_{\mathrm{b2\_n_b}}, \theta_{\mathrm{b2\_n_b}}, \eta_{\mathrm{b2\_n_b}}, \xi_{\mathrm{b2\_n_b}}, \lambda_{\mathrm{b2\_n_b}})^T \\ \dot{\mathbf{u}}_{\mathrm{R}} = \frac{\mathrm{d}\mathbf{u}_{\mathrm{R}}}{\mathrm{d}t}, \quad \dot{\mathbf{u}}_{\mathrm{B1}} = \frac{\mathrm{d}\mathbf{u}_{\mathrm{B1}}}{\mathrm{d}t}, \quad \dot{\mathbf{u}}_{\mathrm{B2}} = \frac{\mathrm{d}\mathbf{u}_{\mathrm{B2}}}{\mathrm{d}t} \end{cases} , \tag{36}$$

where the rotor is supported by asymmetric ball bearings when $\mathbf{u}_{\mathrm{B1}} \neq \mathbf{u}_{\mathrm{B2}}$.

As a result, the total dimensions of generalized vector equal $10 \times n_{\mathrm{s}} + 24 \times n_{\mathrm{b}} + 24 \times 2$. It is clear that the coupled dynamics model of ball bearing–rotor system is much more complicated than simplified spring–rotor dynamic model.

Method and Process to Solve Coupled Dynamic Equations

Figure 8 shows the method and process to solve coupled dynamic equations. They are composed of 5 steps:

(1) Input the system parameters of structure, working condition and lubrication.
(2) Obtain initial displacement and velocity value of rotor and bearings by completing spring–rotor dynamic calculation (ball bearings are equivalent to nonlinear springs) and bearing quasi-static calculation.
(3) Establish the generalized vector of bearing–rotor system by integrating the displacement and velocity vectors and applying constraint equations between rotor and bearings.
(4) Calculated the force and moment vectors of rotor and bearings according to the external loads of rotor and the geometry relationships of bearing parts.
(5) Solve the coupled dynamic equations according to the instantaneous integration method and acquire the dynamic characteristics of bearing–rotor system.

Experiment Verification on the Coupled Dynamic Model

To verify the validity of the coupled dynamic model, the experimental data in the reference [22] are used to compare the numerical results in this paper. Figure 9 shows the angular-contact ball bearing–rotor test rig and the corresponding dynamic model in these literatures. The structural parameters of the bearing–rotor system are shown in Table 1.

The comparison data of the vibration diagram of disk are shown in Fig. 10 in the range of 2000–10,000 rpm. It can be observed that the calculation result of the critical speed in this paper is 3300 rpm, which is very close to the measured value (3280 rpm). The value of amplitude is approximately 360 μm which also has a high consistency with the measured value (about 350 μm).

During the speed range 5400–8400 rpm (90–140 Hz), the vibration waterfall diagram of disk from this paper and the reference [22] are shown in Fig. 11. It can be seen that the frequency components between the numerical results in this paper and the experimental data in the reference [22] are basically similar: the first frequency component (about 54.7 Hz) is related to the first critical speed 3280 rpm; the second frequency component (about 106.7 Hz) corresponds to the resonance frequency which is provoked when the working speed reaches about the double critical speed (6400 rpm).

Furthermore, when the operating speed equals 6400 rpm (mass eccentricity $e = 32$ μm), the spectrums of numerical results and experiment data have a good agreement which is shown in Fig. 12.

Dynamic Characteristics of Asymmetric Ball Bearing–Rotor System

The coupled dynamic model in Fig. 7 is applied to analyze the dynamic features of ball bearing–rotor system. It should be noted that two different ball bearings are used to support the rotor. For this asymmetric bearing–rotor system, the preloading is achieved by applying axial force on the inner rings. The shaft is divided into 10 elements and 11 nodes ($n_{\mathrm{s}} = 11$). The bearings are assembled on the No.2 node and No.10 node. Disk is located on the No.6 node. The variables of structure, material and oil are shown in Table 2.

General Dynamic Features of Asymmetric Ball Bearing–Elastic Rotor System

Dynamic Characteristics of the Elastic Rotor

When the support modes change, the rotor will perform different dynamic features. Under the working conditions that preloading force $F_{pr}=1180$ N, radial load $F_{dr}=5000$ N and axial load $F_{da}=0$ N, the radial vibration diagram of rotor disk is shown in Fig. 13 for both symmetric and asymmetric support. In this way, the influence of different support modes on the rotor vibration in the subcritical region can be obtained.

In Fig. 13, it can be seen that the asymmetrically supported rotors have vibration peaks at 5200 and 4200 rpm, respectively; while, the symmetrically supported rotors only have vibration peaks at 4200 rpm. Moreover, the vibration amplitude of the asymmetrically supported rotor is much smaller than that of the symmetrically supported rotor. The reason can be revealed by the vibration waterfall diagram in the subcritical speed range. The spectrum in the horizontal direction includes 5 frequency components: the VC frequency (the frequency which is caused due to the balls roll in and out of the loading area) and double VC frequency of the left bearing f_{VC1} and $2f_{VC1}$, the VC frequency of right bearing f_{VC2}, the first-order bending resonance frequency f_{xc} and the rotating frequency f_e.

When the rotating speed is about 5400 rpm ($f_{e1}=90$ Hz), $f_{VC1}=(r_{m1}-R_1\cos\alpha_1)\cdot n_{b1}\cdot f_{e1}/d_{m1}=441$ Hz$\approx f_{xc}$ in which r_m is the radius of pitch circle; R is the ball radius; α is the initial contact angle; n_b is the number of balls; f_e is the rotating frequency; d_m is the diameter of pitch circle. The first-order bending mode of the rotor is excited by the VC vibration of the left bearing and the resonance phenomenon occurs. At this time, the vibration amplitude of the disk has a peak value. Similarly, when the speed is about 4200 rpm ($f_{e2}=70$ Hz), $f_{VC2}=(r_{m2}-R_2\cos\alpha_2)\cdot n_{b2}\cdot f_{e2}/d_{m2}=436$ Hz$\approx f_{xc}$, the rotor resonance appears and the vibration amplitude reaches a peak value.

Preload has a significant impact on the dynamic performance of the ball bearing and rotor system. Insufficient preloading force will cause smaller stiffness and higher forced vibration value; excessive preloading force will lead to more increasing wear of structure parts and lower service life.

Therefore, small, moderate and large axial preloading forces (250, 590 and 1180 N) are exerted on the inner rings of both bearings to inspect the preloading effects on the vibration characteristics of the system. Figure 14 shows the horizontal, vertical and axial vibration values of rotor disk in the subcritical speed zone under asymmetric support.

Figure 14a shows that the vibration amplitude in horizontal direction decreases remarkably when the large axial preloading forces are applied on the asymmetric ball bearing–rotor system. It is clear that large preload brings about high stiffness which can reduce vibration intensity.

In Fig. 14b, it can be observed that the increase of preloading force dose not restrain the vertical vibration obviously. The main reason is that the rotor bears a radial load of 5000 N in the vertical direction which is far greater than the preloading force. As a result, the axial preload does not play a leading role in the vertical vibration.

Figure 14c indicates that when preload equals 250 N, axial vibration changes relatively slightly and there is no obvious peak value; when preload is 590 N, the axial vibration appears obvious peak value at 2600 and 3300 rpm, respectively; when preload force is 1180 N, the axial vibration presents obvious peaks at 3400 and 4400 rpm. In a word, when the preload becomes larger, the axial vibration peak will appears at a higher speed. The reason is that the axial natural frequency of the rotor will becomes larger as the preload force rises. Consequently, the rotational speed corresponding to the axial vibration peak will inevitably increase.

To demonstrate the above conclusion, more detailed results about the rotor disk are shown in Fig. 15 at a certain speed (10,000 rpm). It is clear that the radial and axial displacement of rotor disk decreases in Fig. 15a which reveals that the supporting stiffness of bearings increases. Figure 15b shows that the dominate frequency is the rotating frequency (166.7 Hz) and double frequency component (333.3 Hz) also appears in the vertical direction. This is because asymmetric ball bearings will result in different support forces which leads to an additional bending moment. In Fig. 15c, the axial natural frequency of the system changes from 226 to 540 Hz when the preload varies from 250 to 1180 N. It is true that the increase of preloading force can improve the axial supporting stiffness of the rotor and enlarge the axial resonance frequency.

Dynamic Features of the Asymmetric Ball Bearings

To investigate the dynamic features of balls, the displacement, contact angle and relatively sliding speed of corresponding part are shown in Fig. 16.

When preloading force increases, some regular patterns can be observed in Fig. 16: (1) the displacement of balls becomes larger, the amplitude fluctuation becomes smaller and the stationarity of balls is enhanced; (2) the fluctuation of the internal and external contact angles decrease obviously; and (3) the relative sliding speed and fluctuation range between ball and ring raceway are greatly reduced.

Therefore, it is possible to improve stationarity of balls and reduce slip ratio by applying an appropriate preloading force.

On the other hand, the orbits of mass center and the speed fluctuation diagram of cage are shown in Fig. 17 which are used to judge the preload influence on the stability and slip features of cage.

It can be seen in Fig. 17a that the motion of cage center in both bearings fail to form stable circumferential orbits and presents a narrow band-like distribution in a local area when preload force equals 250 and 590 N. It is due to the irregular collision between balls and cage. Moreover, when preload force reaches 1180 N, the orbits of mass center become a stable circumferential whirl. Thus, large preload increases the stationarity and limits the sliding state of ball and reduce the collision between ball and cage. In addition, the outer ring has less guiding force on the oil film of cage, so the movement of cage center tends to be stable.

By comparing the speed fluctuation diagram of Fig. 17b, it can be found that the fluctuation of cage speed becomes smaller when preload force gets bigger. The reason is that the balls become more stable and the collision force with the cage decreases.

Conclusions

This paper provides a dynamic model of typical angular-contact ball bearing–elastic rotor system to study the dynamic characteristics when as asymmetric support mode is used. The conclusions are as follows:

(1) The interactive forces between each part (ball, cage and ring) of the angular-contact ball bearing are obtained by calculating position, velocity and force/moment vector in several founded coordinate systems.
(2) A dynamic model of angular-contact ball bearing–elastic rotor system is presented based on the interactive forces between each part (ball, cage and ring), FEM method to discretize rotor and constraint equations that consolidate rotor and bearing.
(3) The comparison between the numerical results in this paper and experimental data in the corresponding reference verify the validity of the coupled ball bearing–rotor model.
(4) When the system has asymmetric ball bearings, the vibration spectrum of rotor includes the VC frequencies of two bearings, the first-order bending resonance frequency of rotor and the rotating frequency.
(5) When the preload forces of bearings increase, the support stiffness becomes larger and the rotor displacement decreases; moreover, the motions of balls and cage become more stable.

Acknowledgements The work described in this paper is funded by paper was supported by National Key Research and Development Project (2018YFB2000201).

Declarations

Conflict of interest We declare that we do not have any commercial or associative interest that represents a conflict of interest in connection with the work submitted.

References

1. Perret H (1950) Elastiche spielschwingungen konstant belaster walzlger. Werkstatt Betrieb 3:354–358
2. Meldau E (1951) Die Bewegung der Achse von walzlagern bei geringen Drehzahlen. Werkstatt Betrieb 7:308–313
3. Fukata S, Gad EH, Kondou H et al (1985) On the radial vibration of ball bearings: computer simulation. Japan Society of Mechanical Engineers, Tokyo
4. Mevel B, Guyader JL (1993) Routes to chaos in ball bearings. J Sound Vib 162:471–487
5. Harsha SP (2005) Non-linear dynamic response of a balanced rotor supported on rolling element bearings. Mech Syst Signal Process 19:551–578
6. Tiwari M, Gupta K, Prakash O (2000) Dynamic response of an unbalanced rotor supported on ball bearings. J Sound Vib 238:757–779
7. Zhou SY, Shi JJ (2001) Imbalance estimation for speed-varying rigid rotors using time-varying observer. J Dynam Syst Measure Control Trans ASME 123:637–644
8. Harsha SP (2004) The effect of ball size variation on nonlinear vibrations associated with ball bearings. Proc Inst Mech Eng Part K J Multi-Body Dyn 218:191–210
9. Akturk N, Gohar R (1998) The effect of ball size variation on vibrations associated with ball-bearings. Proc Inst Mech Eng Part J J Eng Tribol 212:101–110
10. Akturk N, Uneeb M, Gohar R (1997) The effects of number of balls and preload on vibrations associated with ball bearings. J Tribol 119:747–753
11. Akturk N (1999) The effect of waviness on vibrations associated with ball bearings. J Tribol Trans ASME 121:667–677
12. Aini R, Rahnejat H, Gohar R (1990) A five degrees of freedom analysis of vibrations in precision spindles. Int J Mach Tools Manuf 30:1–18
13. Sunnersjo CS (1978) Varying compliance vibrations of rolling bearings. J Sound Vib 58(3):363–373
14. DeMul JM, Vree JM, Maas DA (1989) Equilibrium and associated load distribution in ball and roller bearings loaded in five degrees of freedom while neglecting friction-part II: application to roller bearings and experimental verification. J Tribol 111(1):149–155
15. Cao Y, Altintas Y (2005) A general method for the modeling of spindle-bearing systems. J Mech Des 126(6):1089–1104
16. Wensing JA (1998) On the dynamics of ball bearings. University of Twente, Netherlands
17. Fritzsn D, Stahl J, Nakhimovski I (2007) Transmission line co-simulation of rolling bearing applications. Linköping University Electronic Press, Linköping, Sweden, pp 24–39
18. Ashtekar A (2012) Experimental and analytical investigation of rotor bearing systems. Dissert Theses Gradworks 48(1):392–397
19. Gupta PK (1984) Advanced dynamics of rolling elements. Springer-Verlag, NewYork

20. Brewe DE, Hamrock BJ (1977) Simplified solution for elliptical-contact deformation between two elastic solids. ASME J Tribol 99:485–487
21. Nelson HD (1980) A finite rotating shaft element using Timoshenko beam theory. J Mech Des Trans ASME 102(4):793–803
22. Bai CQ, Zhang HY, Xu QY (2013) Subharmonic resonance of a symmetric ball bearing-rotor system. Int J Non-Linear Mech 50(1):1–10